Selective cellular imaging with lanthanide based upconversion nanoparticles

DOI:
10.1002/jbio.201800256

Document Version
Accepted author manuscript

Selective cellular imaging with lanthanide based upconversion nanoparticles

Padmaja Parameswaran Nampi[1,*], Alexandre Vakurov[2,3], Lewis E. Mackenzie[2,4], Nigel S. Scrutton[5], Paul A. Millner[2], Gin Jose[1], Sikha Saha[6]

[1]School of Chemical and Process Engineering, Faculty of Engineering, University of Leeds, United Kingdom, LS2 9JT

[2]School of Biomedical Sciences, Faculty of Biological Sciences, University of Leeds, United Kingdom, LS2 9JT ; [3]Present address: School of Chemistry, University of Leeds, United Kingdom, LS2 9JT; [4]Present address: Department of Chemistry, Durham University, Durham, United Kingdom, DH1 3LE

[5]Manchester Institute of Biotechnology (MIB), University of Manchester, United Kingdom, M1 7DN

[6]Leeds Institute for Cardiovascular and Metabolic Medicine (LICAMM), Faculty of Medicine and Health, University of Leeds, United Kingdom, LS2 9JT

*Corresponding Author: Padmaja Parameswaran Nampi, E-mail: p.nampi@leeds.ac.uk

Tel: +44 7438291306

Keywords: nanomaterials, luminescence upconversion, upconversion nanoparticles, toxicity, cellular imaging

Short Title: P.P. Nampi et al. Upconversion nanoparticles for selective cellular imaging

This article has been accepted for publication and undergone full peer review but has not been through the copyediting, typesetting, pagination and proofreading process, which may lead to differences between this version and the Version of Record. Please cite this article as doi: 10.1002/jbio.201800256

Upconversion nanoparticles (UCNPs) with sodium yttrium fluoride, $NaYF_4$ (host lattice) doped with Yb^{3+} (sensitizer) and Er^{3+} (activator), were synthesized via hydrothermal route incorporating polyethyleneimine (PEI) for their long-term stability in water. The cationic PEI modified UCNPs with diameter 20±4 nm showed a zeta potential value of +36.5 mV and showed an intense, visible red luminescence and low intensity green emission with 976 nm laser excitation. The particles proven to be non-toxic to endothelial cells, with an MTT assay, showing 90-100% cell viability, across a wide range of UCNP concentrations (0.3 ng/mL to 0.3 mg/mL) were used in multiphoton imaging. Multiphoton cellular imaging and emission spectroscopy data reported here prove that the UCNPs dispersed in cell culture media are predominantly concentrated in the cytoplasm than the cell nucleus. The radiative energy transfer from PEI coated UCNPs to surrounding media for red luminescence in the biological system is also highlighted with spectroscopic measurements. Results of this study propose that UCNPs can therefore be used for cytoplasm selective imaging together with multiphoton dyes (e.g., DAPI) that are selective to cell nucleus.

1. Introduction

Upconversion is a nonlinear optical process in which multiple photons in the near infrared (NIR) wavelength is absorbed by certain rare earth (RE) doped materials, which then emits photons at visible wavelengths via luminescence [1]. RE doped upconversion nanoparticles (UCNPs) have emerged as a new class of inorganic optical probes that might overcome some of the shortcomings of fluorescent proteins and quantum dots [2]. UCNPs have advantageous properties associated with their infra-red excitation, including low photo-toxicity, no visible auto-fluorescence or photo-bleaching, and excellent photo-stability [3]. The infra-red excitation of UCNPs also enables imaging through up to 2 cm of tissue due to lower scattering and absorption by tissue at these wavelengths [4]. Further, UCNP emission can be tuned by varying elemental composition to enable multiplexed measurement [2, 5, 6-17].

To meet the needs in advanced biomedical and environmental applications, several experimental methods have been developed in order to synthesize UCNPs [18-33]. The hydrothermal method and associated modifications provide several ways to synthesize UCNPs [5-7, 12, 13, 34, 35]. Recently, imaging using luminescent UCNPs as a fluorophore alternative has been reported as a unique approach for visualizing morphological details in tissue at sub cellular resolution with no visible auto-fluorescence, and has become a powerful noninvasive tool for bioimaging [3, 5, 12, 34]. Because of the inherent high photo-stability and non-blinking emission behavior, UCNPs have been shown to enable reliable molecular imaging with long time tracking capability [12, 35]. Zijlmans et al. [36], first exploited the upconversion properties of lanthanide doped particles for high performance bioimaging applications. It has been shown by Yu et al. [37] that upconversion based visualization has negligible fading effect over time. Zhang and Li [37-39] have established UCNPs as luminescent labels for bioimaging in living cells and Prasad et al. [40] reported *in vivo* imaging with Tm^{3+} as well as Yb^{3+} doped nanophosphors. High contrast cellular imaging has been reported using NIR to visible and NIR to NIR UCNPs [38, 41, 42]. Initial attempts have been made in using UCNPs in the imaging of certain cancer cells [38, 41-43].

In the present study, water-dispersible polyethyleneimine (PEI) modified $NaYF_4/Yb^{3+}/Er^{3+}$ UCNPs have been synthesized. In addition to adopting hydrothermal method, the purification process that we followed is important to achieve highly homogeneous aqueous suspension of nanoparticles with less aggregates reported here. The purification involved ultrasonication and redispersion in deionized water followed by filtering through a PD10 column. Although addition of just PEI and use of hydrothermal method have been adopted before, in the present study we have optimised the processing time, purification and dispersion procedures to get a stable suspension, which are very important to get a stable colloidal suspension for further applications. These PEI-modified UCNPs, we prepared in this study, were assessed with respect to size distribution, zeta potential, crystallinity, and luminescence. PEI modified UCNP were used for multiphoton imaging within homogenized liver tissue and endothelial cells. The possible mechanism of luminescent resonance

(LRET) energy transfer which is the reason for variation in fluorescence intensities in the visible spectrum in the biological system is discussed in the paper. We also demonstrated that UCNPs synthesized in this study cause little tissue and cell toxicity and are mainly taken up into the cell cytoplasm. This is promising for site selective imaging applications of PEI modified UCNPs.

2. Experimental Section

Materials: Analytical grade branched PEI [Sigma Aldrich, Molecular weight 25 KDa] and all other reagents including $Y(NO)_3{\cdot}6H_2O$, $Yb(NO)_3{\cdot}5H_2O$, $Er(NO)_3{\cdot}5H_2O$, NH_4F, NaCl, ethylene glycol and acetone, were purchased from Sigma Aldrich. Ultrapure (R =18 MΩ) water was used for final washing of the precipitate and dispersion of the nanoparticles.

2.1. Nanoparticle synthesis: The experimental procedure used for UCNP synthesis was a modification of the synthesis method reported by Zhang et al. [44]. NaCl (10 mmol), $Y(NO)_3{\cdot}6H_2O$ (3.12 mmol), $Yb(NO)_3{\cdot}5H_2O$ (0.8 mmol), $Er(NO)_3{\cdot}5H_2O$ (0.08 mmol) and 1.6 g of PEI were dissolved in 60 ml ethylene glycol (EG) by stirring for 2 h to form a rare earth solution. 16 mmol NH_4F was dissolved in 40 ml of EG was prepared separately and was added to the mixed rare earth solution containing NaCl solution and PEI. The resultant solution was stirred for a further 15 min. The whole mixture was then transferred to a 120 ml Teflon-lined Parr pressure vessel and hydrothermally heated at 200°C for 2 hours. The resultant solution was then allowed to cool down to room temperature and the contents including a very fine precipitate consisting of UCNPs was transferred into a beaker before washing 3-4 times with acetone, and then 4-5 times with ultrapure water by repeated ultracentrifugation at 80000 times gravity for 30 minutes using a Beckman Avanti J20XP high speed centrifuge. The nanoparticle pellet obtained was re-dispersed by sonication using an ultrasonic probe for a maximum of 30 seconds (Bandekin GM2070 with 100% power; cycle 0.7 s). The purified nanoparticles were re-suspended in 4-5 mL of water and passed through a desalting column (PD10, GE Healthcare Life Sciences, Pharmacia Biotech Inc.) to separate the aggregated and finer 'UCNPs'. The following sections exclusively discuss the $NaYF_4/Yb^{3+}/Er^{3+}$ UCNPs

modified with PEI thus obtained.

2.2. Transmission Electron Microscopy and Dynamic Light Scattering (DLS): High resolution transmission electron microscopy of the sample was performed in a TECNAI G^2 High Resolution Field Emission Transmission Electron Microscopy (HRFE-TEM). The sample for the TEM was prepared by placing a drop of UCNPs suspended in water onto the surface of a holey carbon coated Cu grid and letting the water evaporate prior to imaging. The size-distribution of nanoparticles was estimated from TEM images by using a custom MATLAB algorithm (Matlab 2016a), based upon a circular Hough transforms to detect the pseudo-spherical UCNPs [45]. The diameter of the nanoparticle in pixels was subsequently converted to nanometer (nm) by known scale calibration of the HRFE-TEM. Selected area electron diffraction (SAED) was used to verify the lattice planes by comparing with known reference patterns. Energy-dispersive X-ray analysis (EDX) of the sample was also performed during HRFE-TEM to confirm the elemental composition.

DLS was used to ascertain the hydrodynamic diameter and zeta potential of the UCNPs when dispersed in water. Malvern Zetasizer Nano Zs system (Malvern, UK) was used for the DLS measurement.

2.3. X-ray Diffraction (XRD) measurement: XRD measurements of the sample powder obtained by drying the sample at 100°C were made with an X-ray Diffractometer (Bruker D4) using Cu Kα radiation (λ=1.5418 A°) in the 2θ range 10-80° in 0.0247 increments.

2.4. Luminescence emission spectroscopy: In order to measure the luminescence, the sample solution was loaded into 2.0 ml quartz Suprasil cuvettes (Hellma Analytics, UK) placed within a cuvette holder (Qpod 2e, Ocean Optics) at room temperature. The sample was illuminated with a 976 nm near-infrared laser (BL976-PAG900, Thorlabs), operating at a power corresponding to 1000 mA current. UCNP emission was recorded with a high-performance spectrometer (QE-PRO, Ocean Optics) with 1 second integration time and no data averaging.

2.5. *In vitro* endothelial cell culture: Human Umbilical Vein Endothelial Cells (HUVEC, Promocell, UK) were used for the *in vitro* cell study. Passage of cells was carried out by standard

trypsinisation (Sigma Aldrich, UK). After centrifugation, the pellet was re-suspended and cells counted using a haemocytometer. HUVECs (1×10^4) were grown overnight in a 96-well plate. Growth media were prepared using Promocell Endothelial Cell Growth Medium supplemented with Promocell Endothelial cell supplements and 10% (v/v) foetal calf serum and used to feed the growing cells every 2 days until the cells reached ~90% confluency. Media were filtered using Millipore Express (PES) Membranes (pore size 0.22 μm, diam. 33 mm, sterile; γ-irradiated) and Terumo syringes**.**

2.6. *In vitro* cytotoxicity evaluation: The *in vitro* cell viability of UCNPs within endothelial cells was assessed using the 3-(4,5-dimethylthiazol-2yl)-2,5-diphenyltetrazolium bromide (MTT) (Sigma Aldrich) assay. Briefly, 10^4 HUVECs were grown overnight in a 96-well plate. Growth medium were prepared using Promocell Endothelial Cell Growth Medium supplemented with Promocell Endothelial cell supplements and 10% (v/v) foetal calf serum. Increasing doses of nanoparticles from 0.3 ng/mL to 300 μg/mL in growth media were added and incubated for a period of 24 hours. The MTT assay was carried out after 24 hours by adding 50 μL of 5 μg/mL MTT to each well. After the addition of MTT, the plate was incubated for a period of 3 hours, until the purple product appeared. Then, the purple crystals were dissolved using 300 μL/well of isopropanol and plate was read at 576 nm. Cell morphology was observed under light microscope (Olympus BX41) using Cell F imaging software for Life science microscopy in order to examine any change after addition of nanoparticles.

2.7. *In vivo* toxicity testing for liver tissue: All experiments were performed on 10-week-old, 25–30 g male C57BL/6J mice (Harlan-Olac, Bicester, UK), under appropriate United Kingdom Home Office personal and project licenses, adhering to the regulations as specified in the Animals (Scientific Procedures) Act (1986), and according to institutional ethical guidelines. The mice were anaesthetised with isoflurane (1-1.5% in oxygen). The test mice were injected with 100 μl of 0.2 mg/mL of UCNPs in 0.1 M phosphate buffer saline (PBS, pH 7.6) intraperitoneally. Control mice were injected with 100 μl of PBS (pH 7.6). Following 48 hours both experimental and control mice

were perfused transcardially with PBS followed by 4% paraformaldehyde in 0.1 M phosphate buffer (PB, pH 7.4). Liver tissue was harvested and stored in PBS until further processing. For *in vivo* toxicity assessment, part of the liver was fixed in paraformaldehyde and embedded in paraffin using a MEDITE Paraffin Embedding System TES 99, GmbH, Germany. The embedded tissues were cut into thin sections using a Leica RM2235 (Leica Biosystems) rotary microtomes and consequently processed and stained with standard hematoxylin and eosin staining. The histological sections were observed under an Olympus BX41 bright field microscope and the digital images were monitored using Image Pro Plus 7 software (Media Cybernetics) for tissue morphology to establish the non-toxicity of the nanoparticles towards tissues.

2.8. Multiphoton imaging of *ex vivo* liver tissue: Mice were killed by decapitation under anaesthesia (isoflurane, 1-1.5% in oxygen), liver removed and kept in PBS. Part of the liver tissue was cut and homogenised with a blunt needle. 100 μL of the UCNPs (diluted 1μL in 10,000 μL PBS) were added to the tissue and mixed the particles with the tissue by further homogenisation and vortexing. The homogenised tissue with embedded UCNPs was mounted on a slide and air-dried in a refrigerator. The samples were cover slipped using the mounting medium containing DAPI (Vectashield antifade mounting medium with DAPI, Vector Laboratories, UK) viewed under multiphoton microscope.

2.9. Multiphoton imaging of endothelial cells: HUVEC cells were grown on small circular coverslips on an 8 well plate in the exactly the same way as mentioned in the *in vitro* toxicity evaluation measurements. After the cells became confluent, 50 μl of 0.3 ng/mL of nanoparticle solution has been added and incubated for 24 hrs. A coverslip with cells without nanoparticle was used as the control. After incubation the cells are fixed using 70% methanol. The coverslip with samples were mounted on a glass slide with the mounting medium containing DAPI (Vectashield antifade mounting medium with DAPI, Vector Laboratories, UK) and observed under the multiphoton microscope.

Images were acquired using a multiphoton microscope (Upright Zeiss 710; Chemeleon, Coherent, UK) with tunable laser excitation (690 – 1064 nm); 980 nm was selected as it corresponds to peak excitation of $NaYF_4/Yb^{3+}/Er^{3+}$ UCNPs. An external non descanned detector (NDD) was used to acquire Multiphoton images (Carl Zeiss, Germany). Emission spectroscopy analysis of cells was enabled by a spectral detector with photonmultiplier tube (PMT) (Carl Zeiss, Germany). All measurements were acquired at 100% excitation power, corresponding to 180 mW.

3. Results and Discussions

3.1. Transmission Electron Microscopy of UCNPs. HRFE-TEM images of the UCNPs showed a homogeneous distribution with an approximate spherical morphology, with an average particle diameter of 20 ± 4 nm (mean ± standard deviation) (Figure 1a-c). The 2D crystal lattice fringes are visible in Figure 1d; and the distance between the crystal planes are determined to be 3 Å and 2.6 Å, corresponding to the (111) plane and (200) plane respectively [46]. The selected area electron diffraction (SAED) pattern (Figure 1e) demonstrates the highly ordered crystal structure of the UCNPs with the (111), (200) and (220) crystal planes clearly present. From the distance between the crystal planes it can be inferred that UCNPs prepared in this research have α-$NaYF_4$ cubic crystal phase [20]. The energy dispersive X-ray analysis (EDX) spectrum reported in Figure S1 (Supporting Information S1) indicates the molar ratio of the elements Na/Y/Yb/Er/F as 1/0.778/0.210/0.027/4.04 respectively. The concentration of Nitrogen at 0.87 atom percentage indicates the presence of PEI on the surface of the particles.

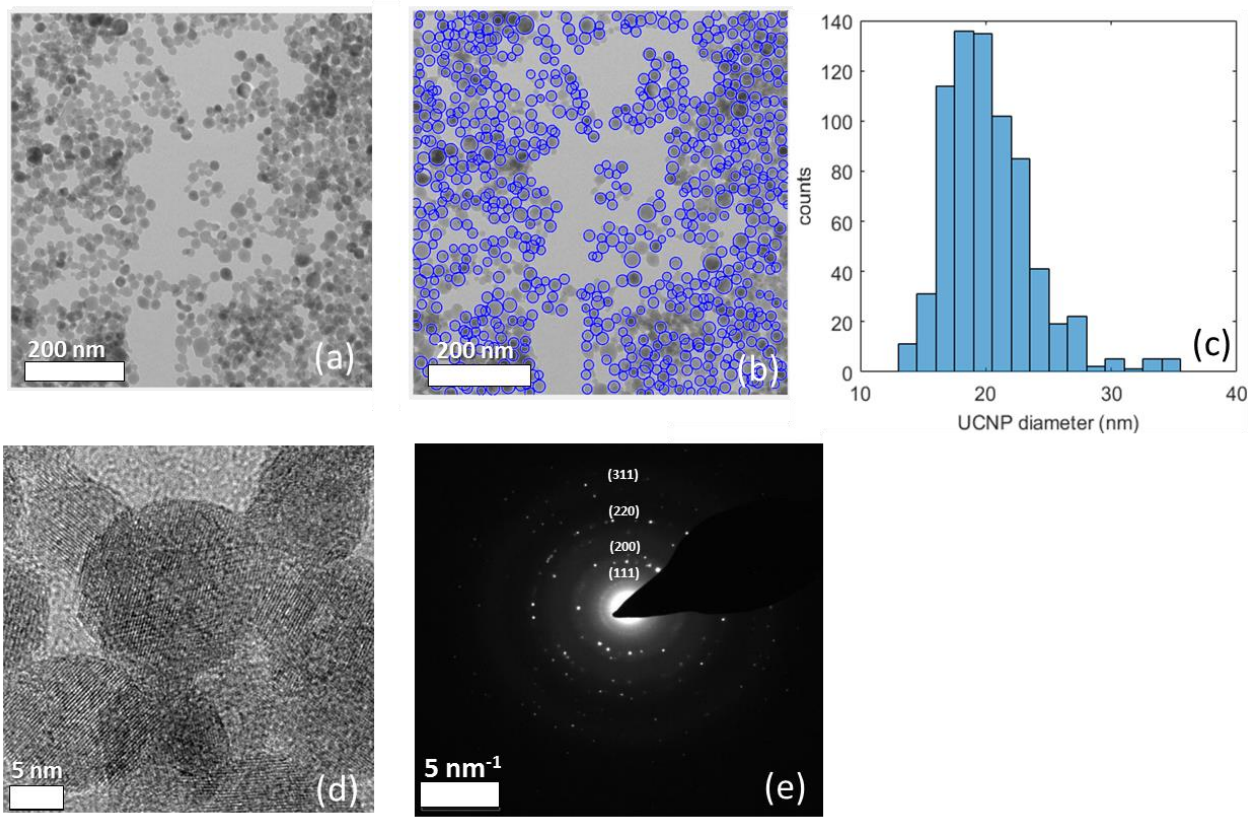

Figure 1 (a) Transmission electron microscopy (TEM) image of the $NaYF_4/Yb^{3+}/Er^{3+}$ UCNPs as synthesized. (b) Detection of UCNPs for size analysis; the blue circles show nanoparticles selected for analysis. (c) Resultant size distribution, showing a normal distribution with an average UCNP diameter of 20 ± 4 nm (mean ± standard deviation). (d) High resolution FE-TEM image of UCNPs. (e) Selected area diffraction pattern demonstrating peaks from UCNP crystal planes.

3.2. X-ray diffraction (XRD) Analysis of UCNPs. The XRD measurements (Figure 2) also confirmed that the crystals are cubic (α-phase) by comparison with the standard test card (JCPDS Card No.77-2042) [20]. The hkl matches with TEM data for the first three planes. From the 2θ peak positions, the cubic lattice parameter, *a* was calculated to be 5.47±0.02 Å (mean ±standard deviation calculated from six individual peaks).

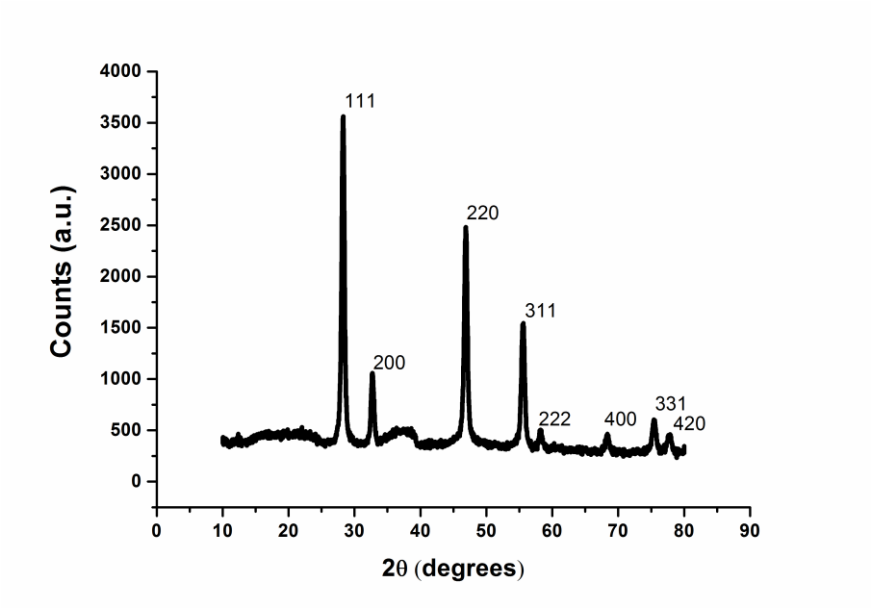

Figure 2 X-ray diffraction pattern of UCNPs. Comparison of the distinct diffraction peaks with known reference shows that the UCNPs are of cubic crystal structure.

3.3. Dynamic Light Scattering Measurements (Particle size in suspension and Zeta potential). Figure 3a and Figure 3b shows the distribution of particles sizes of the UCNPs in solution and the zeta potential measurement respectively, measured using DLS. The particle size distribution

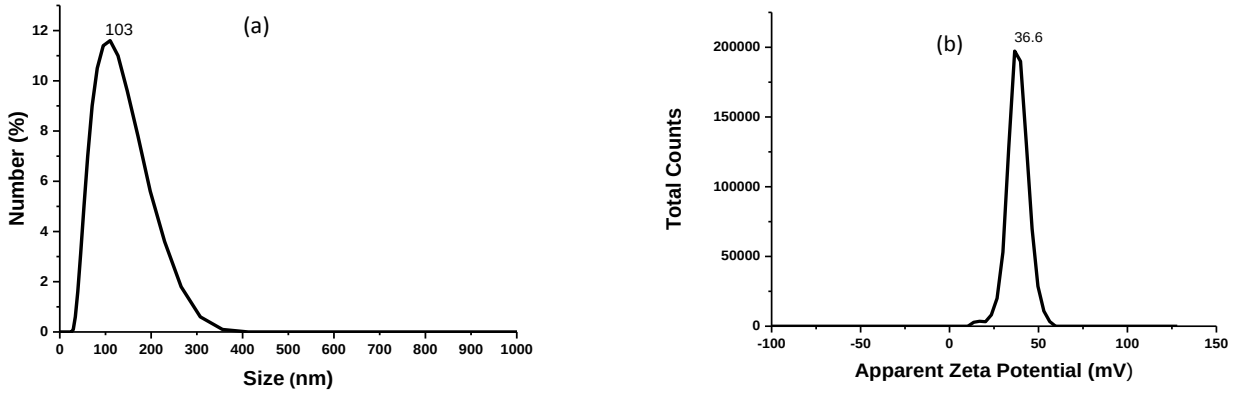

Figure 3 (a) DLS particle size distribution of UCNPs showing maximum particles with mean size corresponding to a hydrophobic diameter of around 100 nm (b) Zeta potential measurement of the UCNPs showing high surface charge.

of the UCNPs by DLS indicated that the maximum particles with mean particle diameter of around 100 nm (Figure 3A). Due to the outer layer of PEI coating on the UCNPs, an increase in hydrodynamic diameter is expected compared to the UCNP size calculated by TEM [44]. Consistent with surface modification by PEI, the PEI-UCNP constructs showed excellent long-term stability in water without any noticeable agglomeration. The long-term water stability makes these PEI-UCNPs suitable for bioimaging applications. The maximum apparent zeta potential value of +36.5 mV, was found to be highly consistent with the isolation of PEI coated UCNPs. The value suggests PEI-UCNPs have cationic surfaces; this can be attributed to the -NH_2 group of the PEI being attached to the particle surface as a hydrophilic head [44]. The positive zeta potential is advantageous for two reason: (1) improved stability in water (2) better cell membrane permeability than negatively charged particles [47]. Thus high zeta potential value is a highly favorable property for tissue and cellular imaging.

3.4. Luminescence emission of UCNPs. Figure 4a shows the homogeneous suspension when not

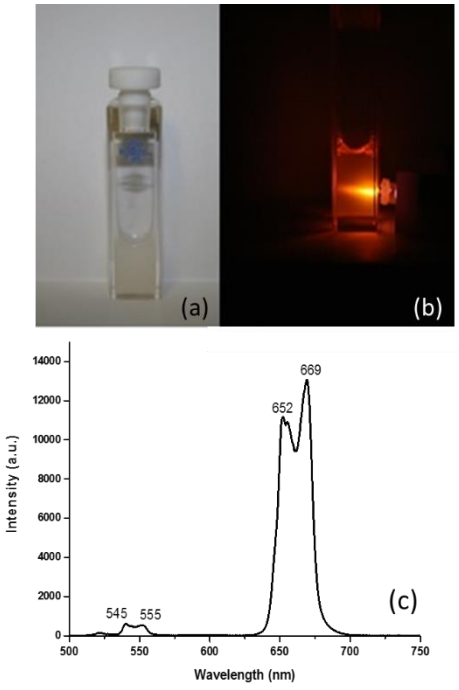

Figure 4 (a) Photograph of the stable UCNP dispersion without excitation in a glass cuvette. (b) UCNP luminescence under 976 nm laser excitation showing orange/red luminescence to the eyes.

(c) Luminescence emission spectrum of UCNPs recorded by a spectrometer showing peaks in the green (~ 540 nm) and red (~660 nm) regions, with the red peak showing considerably greater intensity.

irradiated with 976 nm laser; the white opaque appearance is due to non-absorptive light scattering by the PEI-UCNPs. Under 976 nm illumination UCNPs show apparent orange/red emission visible to the eye (Figure 4b). The UCNP luminescence emission spectrum of the suspension with 976 nm excitation is shown in Figure 4c. The sharp doublet peak in the red wavelength range (635 - 694 nm) is due to the $^4F_{9/2} \rightarrow {}^4I_{15/2}$ transitions, while the weak emission band at 540-560 nm results from the $(^4S_{3/2}, {}^2H_{11/2}) \rightarrow {}^4I_{15/2}$ transitions. The combination of both red and green under 976 nm NIR irradiation results in the deep orange/red emission in the visible light region as shown in Figure 4b.

3.5. *In vitro* cytotoxicity assessment in endothelial cell and *in vivo* liver toxicity assessment.

Cytotoxicity is a concern whenever nanoparticles are applied to the imaging of cells or tissues. An MTT assay was used to assess the cytotoxicity of the UCNPs on human endothelial cells. Co-incubating the cells with UCNPs for 24 hours resulted in average cell viability of 90-100% (Figure 5), indicating that UCNPs are non-toxic to endothelial cells. Further, no change in cell number or morphology was apparent with the maximum concentration of UCNPs (300 μg/ml), indicating good cell viability (Supporting Information Figure S2).

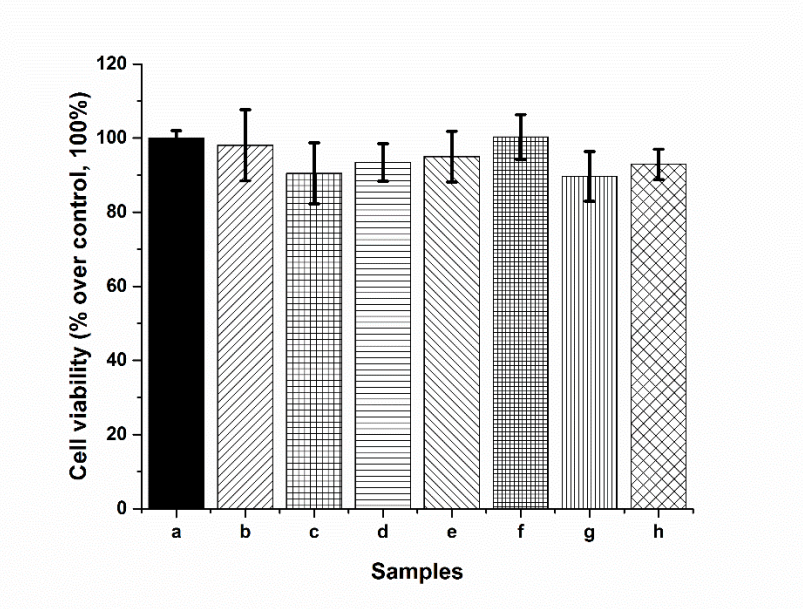

Figure 5 MTT cell viability assay of human endothelial demonstrating the UCNPs are not cytotoxic to endothelial cells. (a) Control (b-h) various concentrations of UCNPs introduced to the sample; 0.3 ng/mL, 3 ng/mL, 30 ng/mL, 300 ng/mL, 3 µg/mL, 30 µg/mL, and 300 µg/mL respectively.

Recent work by Zou et al. indicates that when UCNPs are introduced to mice, the UCNPs accumulated in the liver after 24 hours [48]. In this research *in vivo* toxicity assessment of the UCNPs were carried out in mice. The microscopy images of liver tissue from mice injected with UCNPs and stained with hematoxylin and eosin shown in Figure 6 suggest no apparent tissue damage or lesions in the UCNPs incorporated tissues compared to the control. There was no visible difference in morphology between the control (Figure 6a) and the tissues with the UCNPs (Figure 6b) indicating no apparent toxicity effect of the UCNPs on liver tissues after 48 hours incubation.

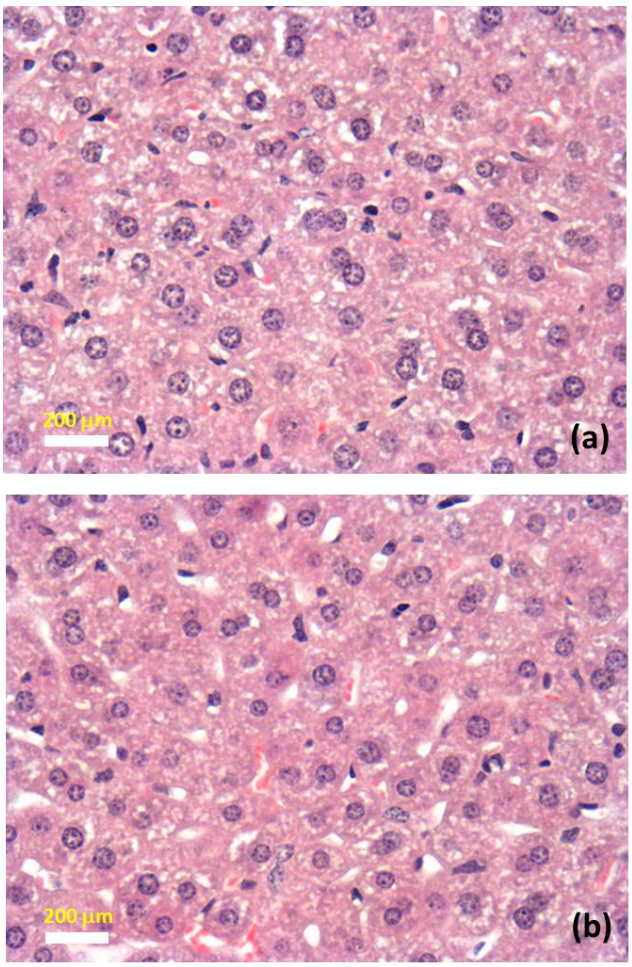

Figure 6 Hematoxylin and eosin stained liver tissue with and without injection of UCNPs. No apparent morphological difference between the control sample (a) and the tissue sample with UCNPs (48 hours post-injection) (b) is evident from the images.

3.6. Multiphoton microscopy of UCNPs within homogenized liver tissue and endothelial cells. Figure 7 shows the multiphoton image of the liver tissue homogenized with the UCNPs, excited at 980 nm. The characteristic green and red emission luminescence spectra of UCNPs was observed in the homogenized liver tissue (see Figure 7b). The spectra are distinct from the typical liver autofluorescence, which under normal ultraviolet or visible excitation is typically a continuous peak ranging from 400-650 nm [49]. Note, the sharp peaks of UCNPs are not clearly resolved in Figure 7b due to the low spectral sampling resolution of the multiphoton microscope (approximately 10 nm).

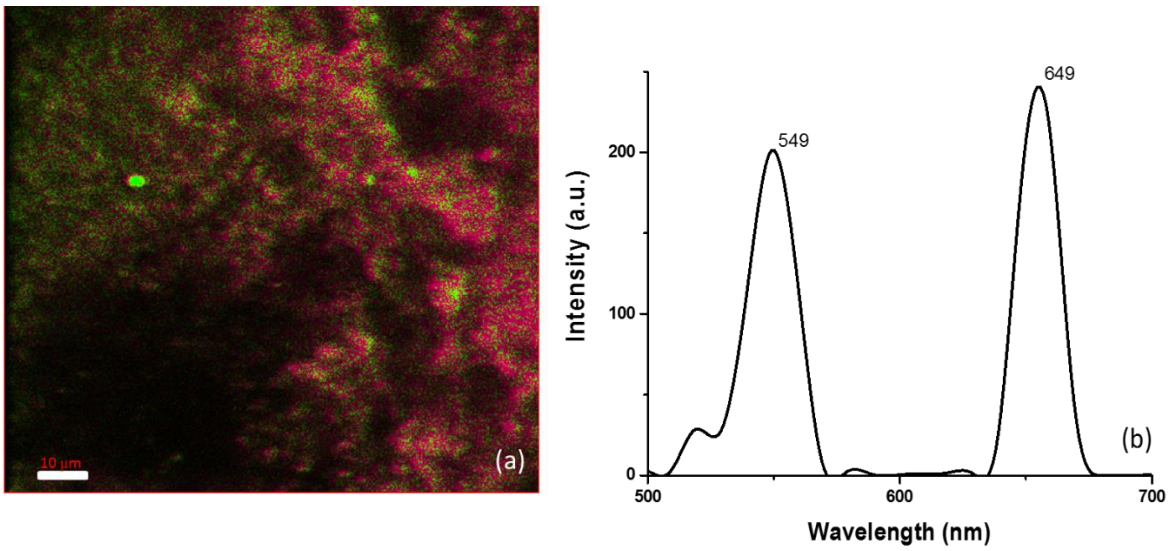

Figure 7 (a) Multiphoton image of the homogenized mouse liver tissue with UCNPs after 48 hours incubation, excited at 980 nm. The reason for spatial distribution of red and green emission is currently unclear. (b) Representative λ-scan emission spectrum of the corresponding image at 980 nm excitation clearly showing the characteristic green and red luminescence peaks of UCNPs.

The spectral emission data of UCNPs in tissue shows a pseudo-uniform distribution of particles in the homogenized tissue. The red emission peak was greatly reduced compared to the UCNPs in as-prepared solution (see Figure 4c) suggesting red emission quenching in Figure 7b is due to a localized interaction between the UCNPs and molecular constituents of liver tissues. The peak intensity ratio of red to green is 24.3 for UCNPs in solution while that in liver tissues is 1.03. The UCNP emission ratio between red and green is also non-uniform across the homogenized tissue sample though there is a drop in red intensity in comparison to green everywhere. The reason for this is due to localized interactions between the UCNPs and the variations in the molecular sites in the homogenized tissue that is attached to the UCNPs, resulting energy loss from the UCNPs via luminescence resonance energy transfer (LRET) identical to that observed in rare earth complexes [50]. This data supports that UCNPs are suitable for tissue imaging without autofluorescence.

Study has also been conducted to see the interaction and uptake of UCNPs by endothelial cells. Figure 8a shows the multiphoton image of the endothelial cells with mounting medium containing

DAPI and UCNPs when excited at 760 nm. The image clearly shows only the DAPI stained cell nucleus at this excitation wavelength. Figure 8b showed the overlay images obtained at 760 nm and 980 nm respectively. It can be clearly seen that the particles are predominantly attached to the cells around the nucleus and the cell morphology is not affected. This is consistent with the previous observation [51].

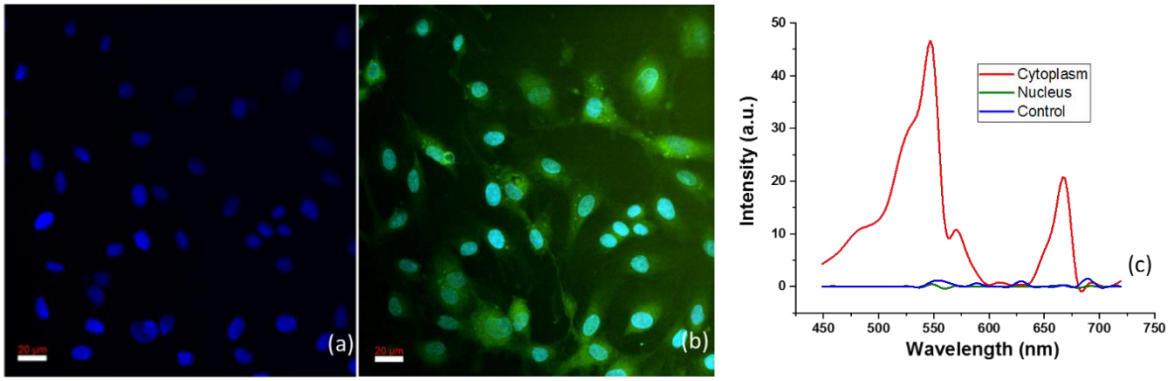

Figure 8 Multiphoton images of DAPI stained endothelial cells with low concentration of nanoparticles (0.3 ng/mL) added and subsequently incubated for 24 hours. (a) 760 nm excitation, highlighting the DAPI stained cell nucleus only. (b) 980 nm excitation image of excited UCNPs overlaid upon (a) showing apparent UCNP emission from cytoplasm. (c) λ-curve showing the wavelength of emission from the cytoplasm and nucleus at 980 nm and control cells.

In order to confirm the origin of the intense green emission the spectra were recorded from various locations within the cell media and reported in Figure 8c. The spectrum recorded in the cytoplasm clearly shows characteristic dual-emission peak of UCNPs, whereas the nucleus shows no emission, indicating UCNPs are only absorbed into the cytoplasm and not into the nucleus. Figure 8b and 8c show that UCNPs are localised in the cytoplasm but not in the nucleus. This clearly demonstrates the importance of UCNPs in the selective multiphoton imaging of cellular cytoplasm. The wavelengths of emission from the cytoplasm (Fig. 8d) also shows relatively higher emission intensity in the green region than the red region. The ratio of red to green (R/G) peak intensity in this spectrum is 0.18 which is significantly lower than that of UCNPs in solvent reported in figure

4b. The quenching of red emission could be attributed to the LRET from the UCNPs to the cellular proteins, located within 20 nm of UCNPs similar to that described above for UCNPs in liver tissues. However in both cases for a detailed understanding of the LRET requires knowledge of the molecules in the biological media that preferentially attach to UCNPs and time resolved spectroscopic studies. Figure 8 also demonstrate DAPI can be used in conjunction with UCNPs for dual wavelength excitation for selective imaging of nucleus and cytoplasm respectively. Results reported here is promising for using the PEI coated UCNPs safely in multiphoton bioimaging applications with multiple wavelength imaging modality.

4. Conclusions

PEI modified $NaYF_4/Yb^{3+}/Er^{3+}$ UCNPs were synthesized by a novel hydrothermal method. HRFE-TEM showed particles with a mean diameter of 20±4 nm, and an overall diameter range between 10-35 nm. Measurements with DLS indicated a much wider diameter distribution when in solution, with a mean nanoparticle diameter of ~100 nm due to the hydrated PEI outer layer. The UCNP zeta potential value of +36.5 mV indicates the cationic surface of the particles and PEI modification increased the water stability of the nanoparticles; an important parameter for cellular uptake in bioimaging applications. The non-toxicity of the particles towards liver tissue and endothelial cells was confirmed by hematoxylin and eosin staining, and MTT assays respectively. Imaging of UCNPs in presence of homogenized liver tissue exhibited the characteristic luminescence spectra of UCNPs, indicating that UCNPs can be used for tissue imaging without background tissue autofluorescence. Multiphoton imaging and emission spectroscopy of endothelial cell utilizing UCNPs indicated that UCNPs are absorbed into the cytoplasm, but not the nucleus. This indicates that UCNPs are suitable for cell structure applications, and that our PEI-modified UCNPs were uptaken into the cytoplasm specifically. This initial study demonstrates that in future UCNPs could be applied to bioimaging of cell structures and tissue imaging. LRET which is the main cause of drop in luminescence intensity of red relative to green for UCNPs in biological media is observed in this research. With appropriate surface modification and suitable bioconjugation procedures, UCNPs could be utilized for targeted

imaging and as biosensors for sensing of biomolecules and proteins.

Supporting Information

Additional supporting information may be found in the online version of this article at the publisher's website.

Acknowledgments

The Corresponding Author Padmaja Parameswaran Nampi (PPN), Marie Skłodowska-Curie Experienced Researcher has received funding from the European Commission Horizon 2020 Framework Programme – H2020 Marie Skłodowska-Curie Actions under the Grant Agreement No. 707297. PPN would like to thank Hema Viswambharan for her guidance on HUVECs culture and stimulation. PPN acknowledges Nadira Yuldasheva and Nicole Conway for their technical support in light microscopic tissue preparation and staining. PPN acknowledges British Heart Foundation, Wellcome Trust and University of Leeds, UK for having the Multiphoton Fluorescence Laser Imaging Facility in LICAMM, used for this research work. PPN acknowledges David Myers for helping with the multiphoton imaging tasks. Lewis E. Mackenzie was funded by a grant from the Biotechnology and Biological Sciences Research Council Tools and Resources Development Fund (BBSRC, TRDF). Alexandre Vakurov was funded by Natural Environment Research Council, the UK. Nigel Scrutton is an EPSRC Established Career Fellow.

References

[1] F. Auzel, Chem. Rev., 2004, **104,** 139-173.

[2] F. Wang, D. Banerjee, Y. S. Liu, X. Y. Chen and X. G. Liu, Analyst, 2010, **135,** 1839-1854.

[3] J. J. Zhou, S. Q. Xu, J. J. Zhang and J. R. Qiu, Nanoscale, 2015, **7,** 15026-15036.

[4] Q. Liu, Y. Sun T. Yang, W. Feng, C. Li and F. Li, J. Am. Ceram. Soc., 2011, **133,** 17122-17125.

[5] M. G.–Bejar, L. F.–Sariano and J. P. -Perieto, Front. Bioeng. Biotechnol., 2016**, 4,** 1-9.

[6] D. K. Chatterjee and M. K. Gnanasammandhan, Y. Zhang, Small, 2010, **6,** 2781-2795.

[7] M. Haase and H. Schafer, Angew. Chem. Int. Edn., 2011, **50,** 5808-5829.

[8] X. M. Li, F. Zhang and D. Y. Zhao, Nano Today, 2013, **8,** 643-676.

[9] B. Zhou, B. Y. Shi, D. Y. Jin and X. G. Liu, Nat. Nanotechnol., 2015, **10,** 924-936.

[10] X. G. Liu, C. H. Yan and J. A. Capobianco, Chem. Soc. Rev., 2015, **44,** 1299-1301.

[11] H. Dong, L. D. Sun and C. H. Yan, Nanoscale, 2013, **5,** 5703-5714.

[12] G. Y. Chen, H. L. Qiu and P. N. Prasad, X. Y. Chen, Chem. Rev., 2014, **114,** 5161-5214.

[13] Z. J. Li, Y. W. Zhang, H. E. La, R. Zhu, G. El-Banna, Y. Z. Wei and G. Han, Nanomaterials-Basel, 2015, **5,** 2148-2168.

[14] C. Bouzigues, T. Gacoin and A. Alexandrou, Acs Nano, 2011, **5,** 8488-8505.

[15] M. V. DaCosta, S. Doughan, Y. Han and U. J. Krull, Anal. Chim. Acta, 2014, **832,** 1-33.

[16] L. Y. Ang, M. E. Lim, L. C. Ong and Y. Zhang, Nanomedicine-UK, 2011, **6,** 1273-1288.

[17] D. Yang, P. Ma, Z. Hou, Z. Cheng, C. Li and J. Lin, Chem. Soc. Rev., 2015, **44,** 1416-1448.

[18] G. S. Yi, H. C. Lu, S. Y. Zhao, G. Yue, W. J. Yang, D. P. Chen and L. H. Guo, Nano Lett., 2004, **4,** 2191-2196.

[19] Y. Wei, F. Q. Lu, X. R. Zhang and D. P. Chen, Chem. Mater., 2006, **18,** 5733-5737.

[20] H. X. Mai, Y. W. Zhang, R. Si, Z. G. Yan, L. D. Sun, L. P. You and C. H. Yan, J. Am. Chem. Soc., 2006, **128,** 6426-6436.

[21] J. C. Boyer, F. Vetrone, L. A. Cuccia and J. A. Capobianco, J. Am. Chem. Soc., 2006, **128,** 7444-7445.

[22] G. S. Yi and G. M. Chow, Adv. Funct. Mater., 2006, **16,** 2324-2329.

[23] S. Mishra, S. Daniele, G. Ledoux, E. Jeanneau and M. F. Joubert, Chem. Commun., 2010, **46,** 3756-3758.

[24] W. B. Niu, S. L. Wu, S. F. Zhang and L. Li, Chem. Commun., 2010, **46 (22),** 3908-3910.

[25] H. Schafer, P. Ptacek, H. Eickmeier and M. Haase, Adv. Funct. Mater., 2009, **19,** 3091-3097.

[26] Z. Q. Li and Y. Zhang, Nanotechnology, 2008, **19,** 345606-345610.

[27] X. M. Liu, J. W. Zhao, Y. J. Sun, K. Song, Y. Yu, C. A. Du, X. G. Kong and H. Zhang, Chem. Commun., 2009, **43,** 6628-6630.

[28] Y. A. Yang, O. Chen, A. Angerhofer and Y. C. Cao, J. Am. Chem. Soc., 2006, **128,** 12428-12429.

[29] S. H. Tang, J. N. Wang, C. X. Yang, L. X. Dong, D. L. Kong and X. P. Yan, Nanoscale, 2014, **6,** 8037-8044.

[30] S. F. Lim, R. Riehn, C. K. Tung, W. S. Ryu, R. Zhuo, J. Dalland and R. H. Austin, Nanotechnology, 2009, **20,** 405701-405706.

[31] M. Pires, O. A. Serra and M. R. Davolos, J. Lumin., 2005, **113,** 174-182.

[32] X. Qin, T. Yokomori and Y. G. Ju, Appl. Phys. Lett., 2007, **90,** 073104-073106.

[33] Y. L. Hu, B. Y. Wu, Q. Jin, X. Y. Wang, Y. Li, Y. X. Sun, J. Z. Huo and H. J. Zhao, Talanta, 2016, **152,** 504-512.

[34] M. Lin, Y. Zhao, S. Q. Wang, M. Liu, Z. F. Duan, Y. M. Chen, F. Li and F. Xu, Biotechnol. Adv., 2012, **30,** 1551-1561.

[35] D. Ostrowski, E. M. Chan, D. J. Gargas, E. M. Katz, G. Han, P. J. Schuck, D. J. Milliron and B. E. Cohen, Acs Nano, 2012, **6,** 2686-2692.

[36] H. J. Zijlmans, J. Bonnet, J. Burton, K. Kardos, T. Vail, R. S. Niedbala and H. J. Tanke, Anal. Biochem., 1999, **267,** 30-36.

[37] M. X Yu, F. Y.Li, Z. G Chen, H.Hu, - C. Zhan, -H. Yang and C. H. Huang, Anal. Chem., 2009, **81,** 930-935.

[38] D. K. Chatterjee, A. J. Rufalhah and Y. Zhang, Biomaterials, 2008, **29,** 937-943

[39] L. Q. Xiong, Z. G. Chen, M. X. Yu, F. Y. Li, C. Liu and C. H. Huang, Biomaterials, 2009, **30,** 5592-5600.

[40] M. Nyk, R. Kumar, T. Y. Ohulchanskyy, E. J. Bergey and P. N. Prasad, Nano. Lett., 2008, **8,** 3834-3838.

[41] F. Vetrone, R. Naccache, A. J. de la Fuente, F. Sanz-Rodriguez, A. Blazquez-Castro, E. M. Rodriguez, D. Jaque, J. G. Sole and J. A. Capobianco, Nanoscale, 2010, **2,** 495-498.

[42] B. Sikora, K. Fronc, I. Kaminska, K. Koper, S. Szewczyk, B. Paterczyk, T. Wojciechowski, K. Sobczak, R. Minikayev, W. Paszkowicz, P. Stepien and D. Elbaum, Nanotechnology, 2013, **24,** 235702-235712.

[43] Y. Yang, Y. Han and C. Yue, Nano. Biomed. Eng., 2016, **8,** 161-171.

[44] S. Zhang, J. Wang, W. Xu, B. T. Chen, W. Yu, L. Xu and H. W. Song, J. Lumin., 2014**, 147,** 278-283.

[45] L. E. Mackenzie, J. A. Goode, A. Vakurov, P. P. Nampi, S. Saha, G. Jose and P. A. Millner Sci. Rep., 2018, **8 (1)** DOI:10.1038/s41598-018-19415-w

[46] J. F. Jin, Y. J. Gu, C. W. Y. Man, J. P. Cheng, Z. H. Xu, Y. Zhang, H. S. Wang, V. H. Y. Lee, S. H. Cheng and W. T. Wong, Acs Nano, 2011, **5,** 7838-7847

[47] O. S. Wolfbeis, Chem. Soc. Rev., 2015, **44,** 4743-4668.

[48] R. Zou, J. Huang, J. Shi, L. Huang, X. Zhang, K. Wong, H. Zhang, D. Jin, J. Wang and Q. Su, Nano. Res., 2017, **10,** 2070-2082.

[49] C. Croce, A. Ferrigno, G. Santin, V. M. Piccolini, G. Bottiroli and M. Vairetti, Laser Surg. Med., 2014, **46,** 412-421.

[50] H. E. Rajapaksea , N. Gahlauta , S. Mohandessia , D. Yub , J. R. Turnerb , and L. W. Millera, PNAS, 2010, 107, 13582-13587.

[51] D. H. M. Dam, J. H. Lee, P. N. Sisco, D. T. Co, M. Zhang, M. R. Wasielewski and T. W. Odom, Acs Nano, 2012, **6,** 3318-3326.

Graphical Abstract for Table of Contents (TOC)

Selective cellular imaging with lanthanide based upconversion nanoparticles

Padmaja Parameswaran Nampi*, Alexandre Vakurov, Lewis E. Mackenzie, Nigel S. Scrutton, Paul A. Millner, Gin Jose, Sikha Saha

Highly fluorescent water dispersible polyethyleneimine coated $NaYF_4/Yb^{3+}/Er^{3+}$ upconversion nanoparticles synthesized using hydrothermal method are promising non-toxic biocompatible materials for imaging cellular cytoplasm.